Electronic Supplementary Information

Effective Production of Liquid/Wax Fuels from Polyethylene Plastics Using Ru/Al_2O_3 Catalysts

Jueun Kim,‡[a] Donghyeon Kim,‡[b] Byung Gwan Park,[a] Daewon Oh,[a] Shinjae Lee,[a] Jihun Kim,[a] Eonu Nam,[a] and Kwangjin An*[a,b]

[a]School of Energy and Chemical Engineering, and Graduate School of Carbon Neutrality, Ulsan National Institute of Science and Technology (UNIST), Ulsan 44919, Republic of Korea. a.

[b]School of Carbon Neutrality, Ulsan National Institute of Science and Technology (UNIST), Ulsan 44919, Republic of Korea.

‡These authors contributed equally to this work.

*To whom correspondence should be addressed (E-mail: kjan@unist.ac.kr)

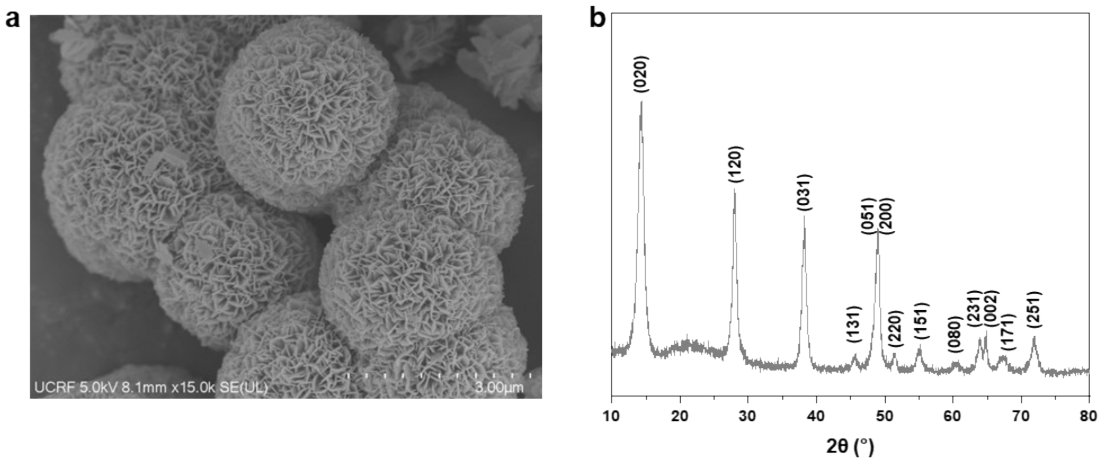

Fig. S1 SEM image and XRD pattern. (a) SEM image and (b) XRD pattern (JCPDS 21-1307) of as-prepared NA-AlOOH.

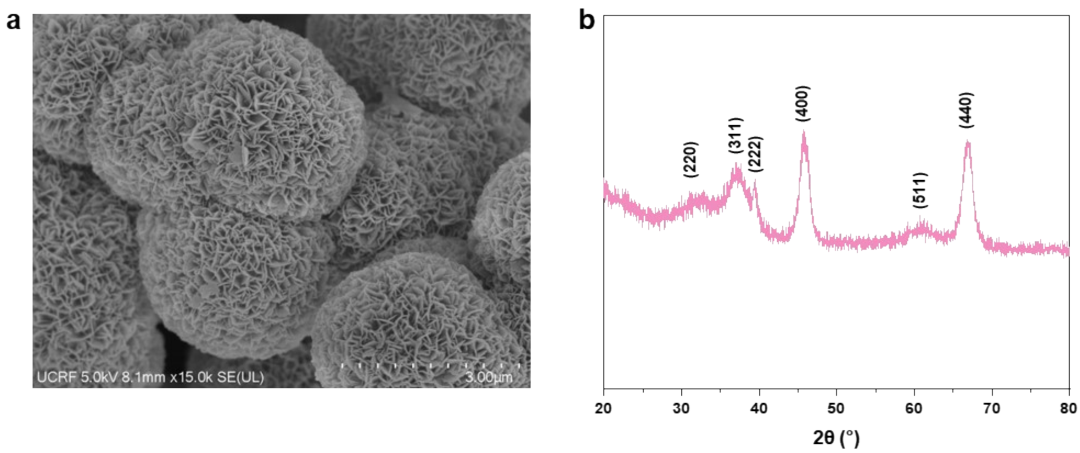

Fig. S2 SEM image and XRD pattern. (a) SEM image and (b) XRD pattern (JCPDS 29-0063) of NA-Al_2O_3.

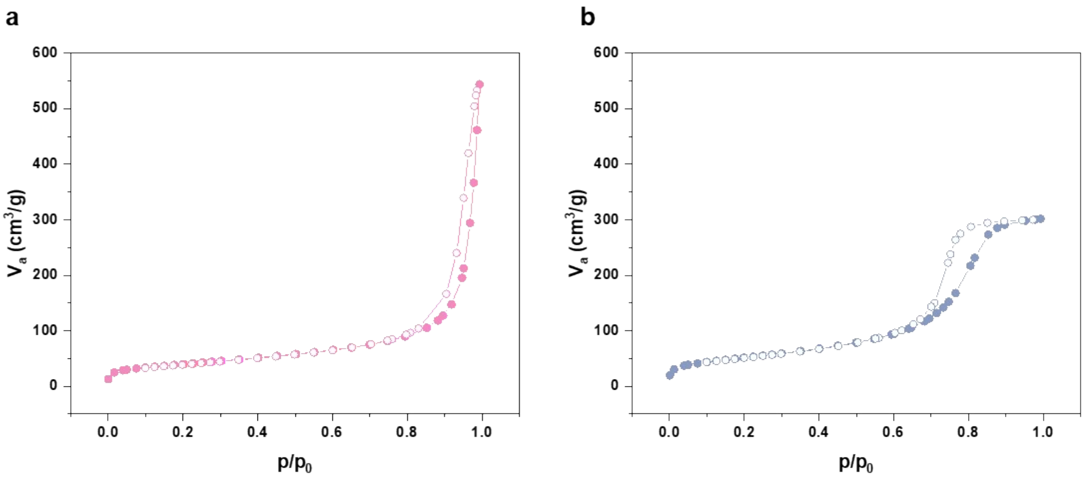

Fig. S3 N_2 adsorption-desorption isotherms. (a) NA-Al_2O_3 and (b) *com*-Al_2O_3.

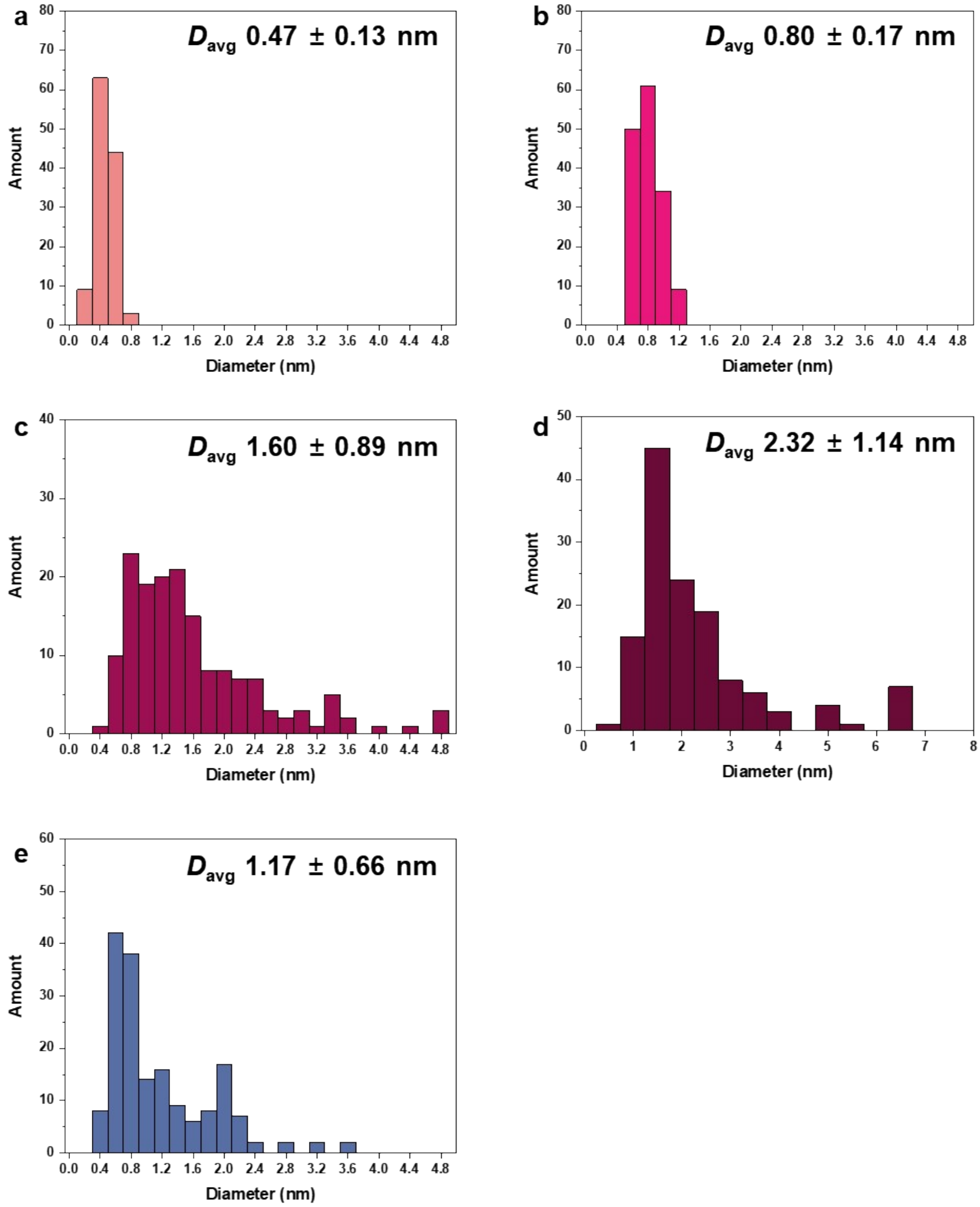

Fig. S4 Particle size distributions of Ru/Al_2O_3 catalysts. (a) 0.5Ru/NA-Al_2O_3, (b)1Ru/NA-Al_2O_3, (c) 5Ru/NA-Al_2O_3, (d) 8Ru/NA-Al_2O_3, and (e) 1Ru/*com*-Al_2O_3.

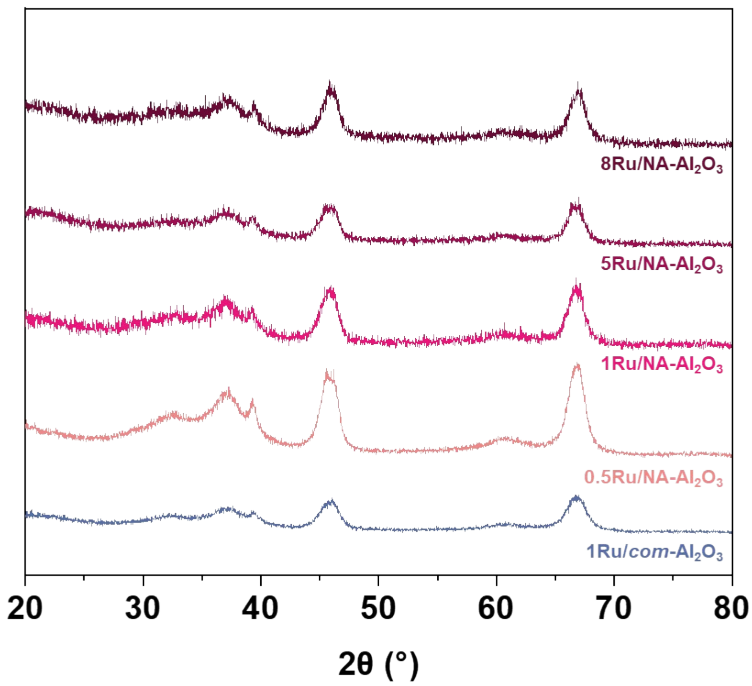

Fig. S5 XRD patterns of Ru/Al_2O_3 catalysts.

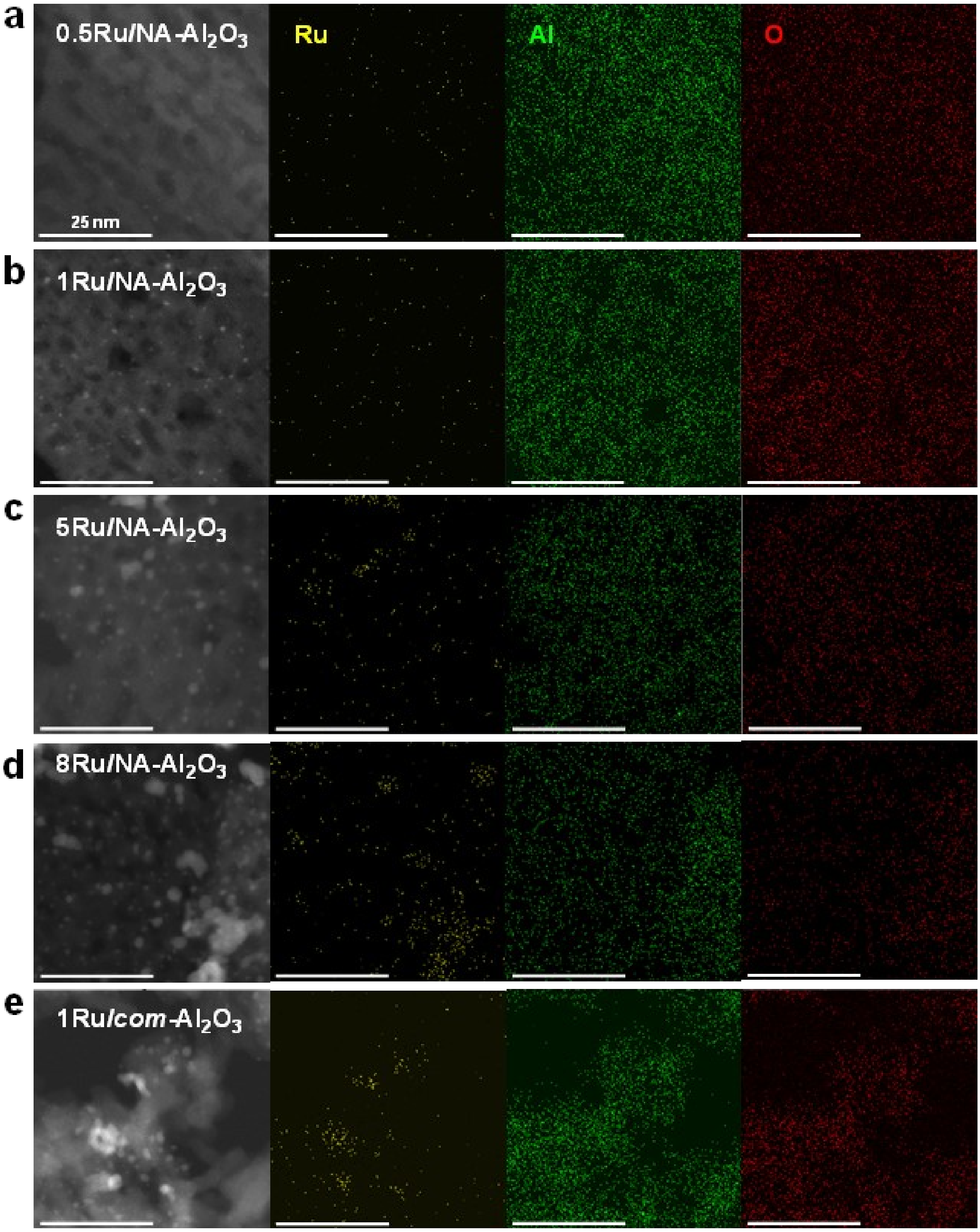

Fig. S6 HAADF-STEM images and EDS elemental mappings of Ru/Al_2O_3 catalysts. (a) 0.5Ru/NA-Al_2O_3, (b) 1Ru/NA-Al_2O_3, (c) 5Ru/NA-Al_2O_3, (d) 8Ru/NA-Al_2O_3, and (e) 1Ru/*com*-Al_2O_3.

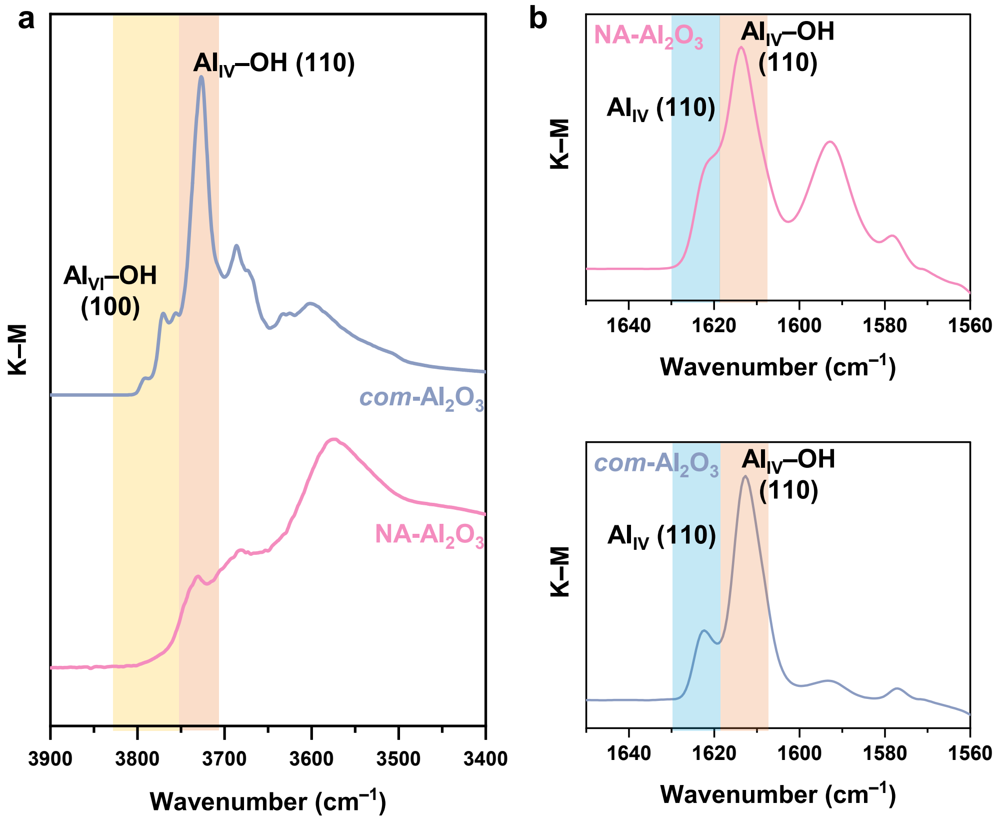

Fig. S7 DRIFT spectra presented using the Kubelka–Munk (K–M) function. (a) *In situ* DRIFT spectra in OH stretching regions of NA-Al_2O_3 and *com*-Al_2O_3 at 25 °C. (b) Pyridine adsorbed DRIFT of NA-Al_2O_3 and *com*-Al_2O_3 at 100 °C (Normalized with the intensity of 1613 cm^{-1}).

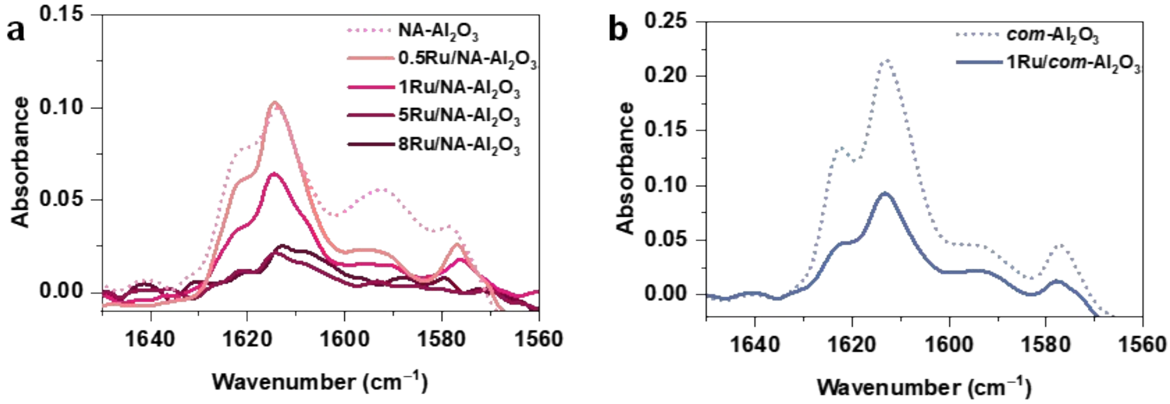

Fig. S8 Pyridine-adsorbed DRIFT at 1650–1560 cm^{-1} of Ru/Al_2O_3 catalysts. (a) xRu/NA-Al_2O_3 and (b) 1Ru/*com*-Al_2O_3.

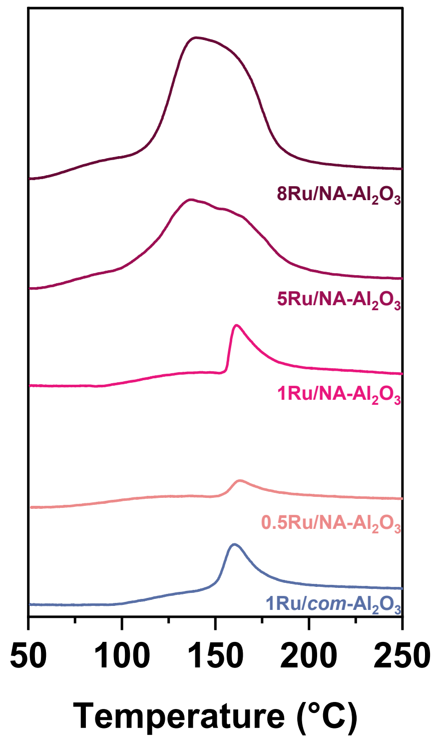

Fig. S9 H_2-TPR of the as-prepared Ru catalysts.

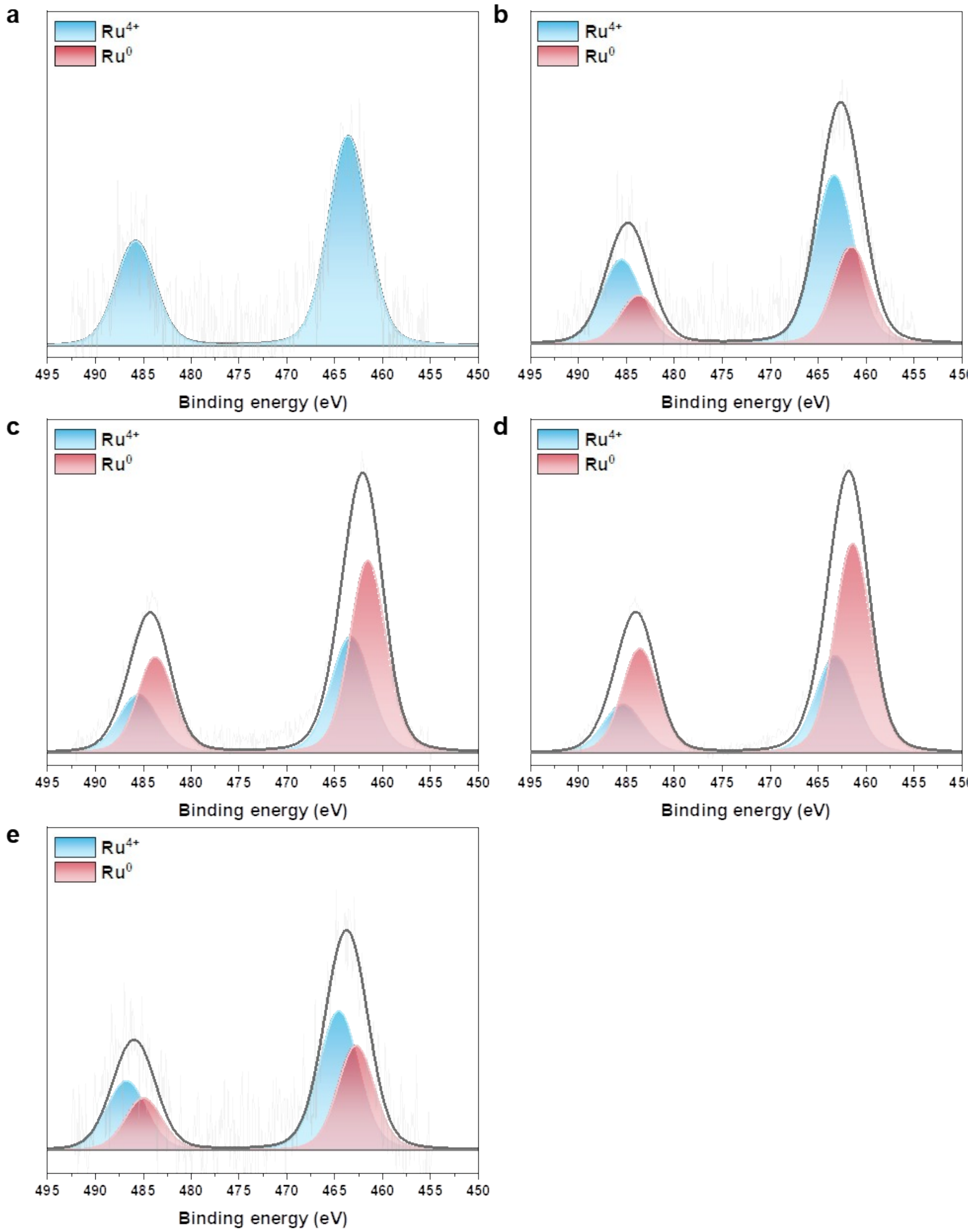

Fig. S10 XPS profiles of Ru/Al_2O_3 catalysts. (a) $0.5Ru/NA\text{-}Al_2O_3$, (b) $1Ru/NA\text{-}Al_2O_3$, (c) $5Ru/NA\text{-}Al_2O_3$, (d) $8Ru/NA\text{-}Al_2O_3$. and (e) 1Ru/*com*-Al_2O_3.

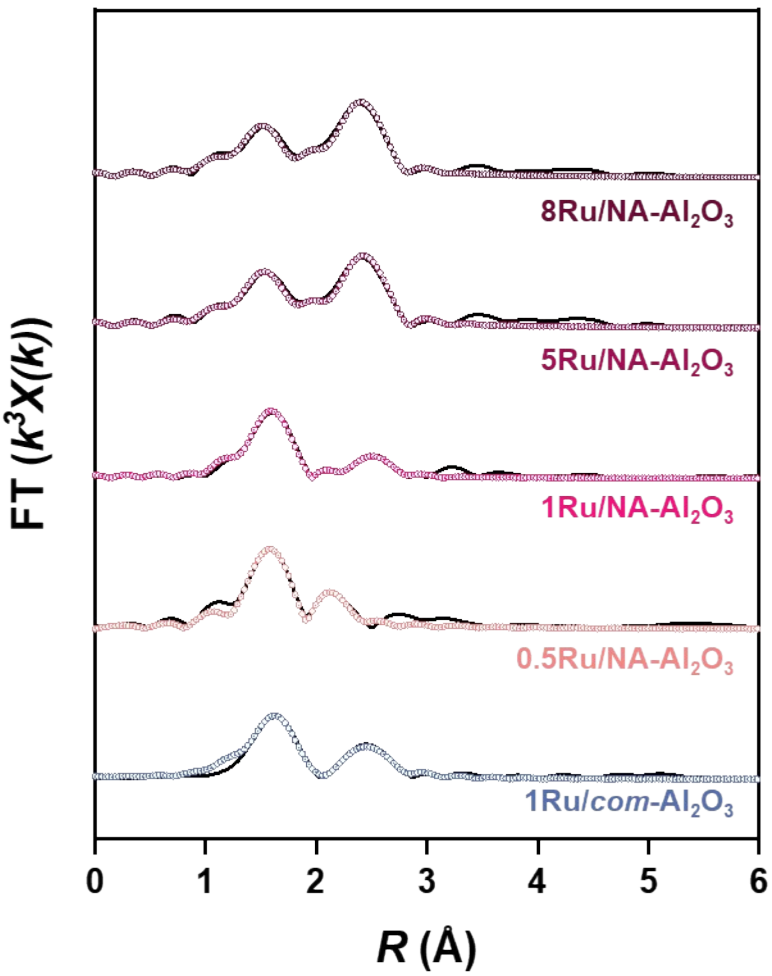

Fig. S11 Ru *K*-edge EXAFS *R*-space spectra and their fitting of Ru/Al_2O_3 catalysts.

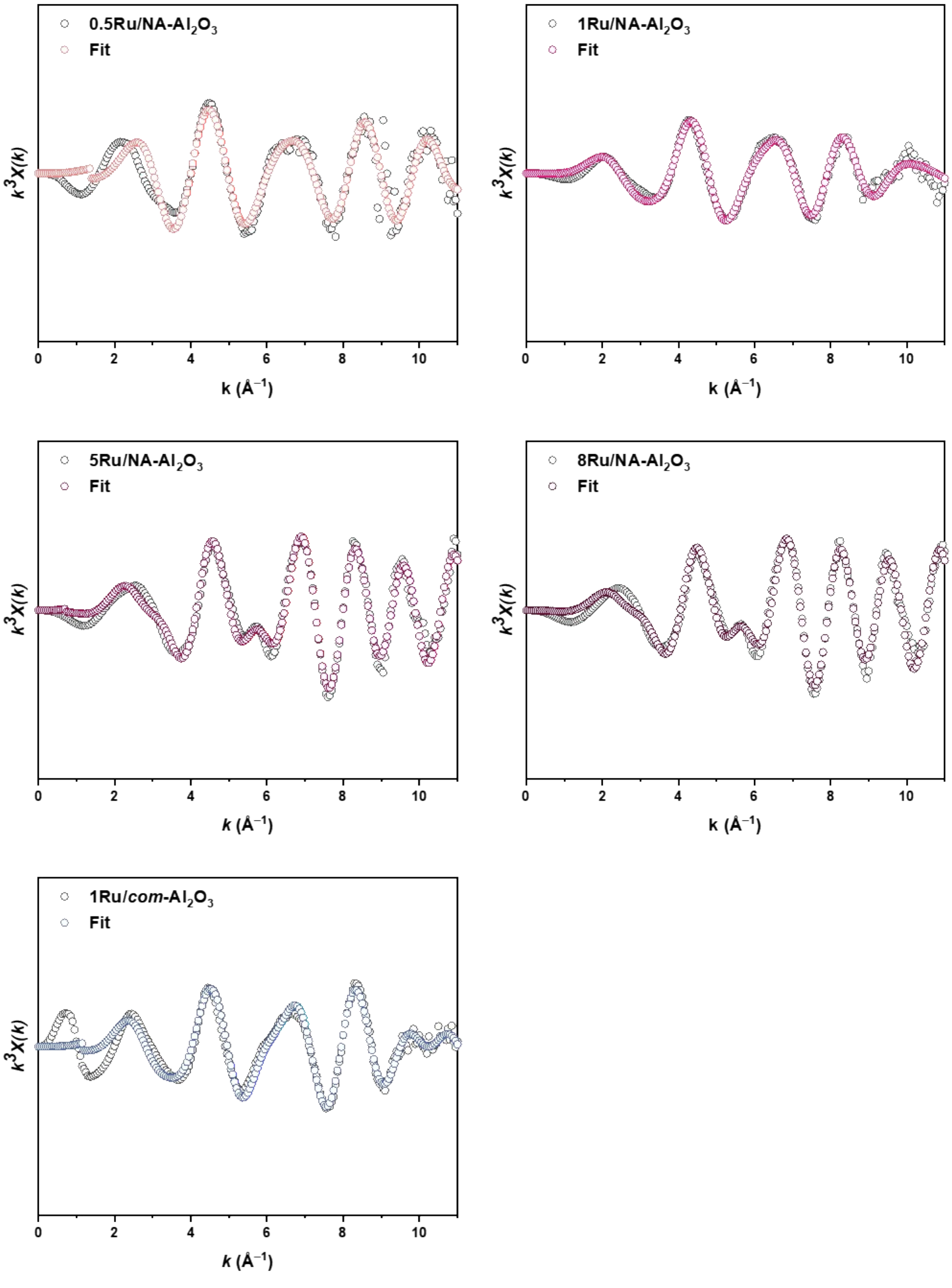

Fig. S12 Ru *K*-edge EXAFS *k*-space spectra and their fitting of Ru/Al_2O_3 catalysts.

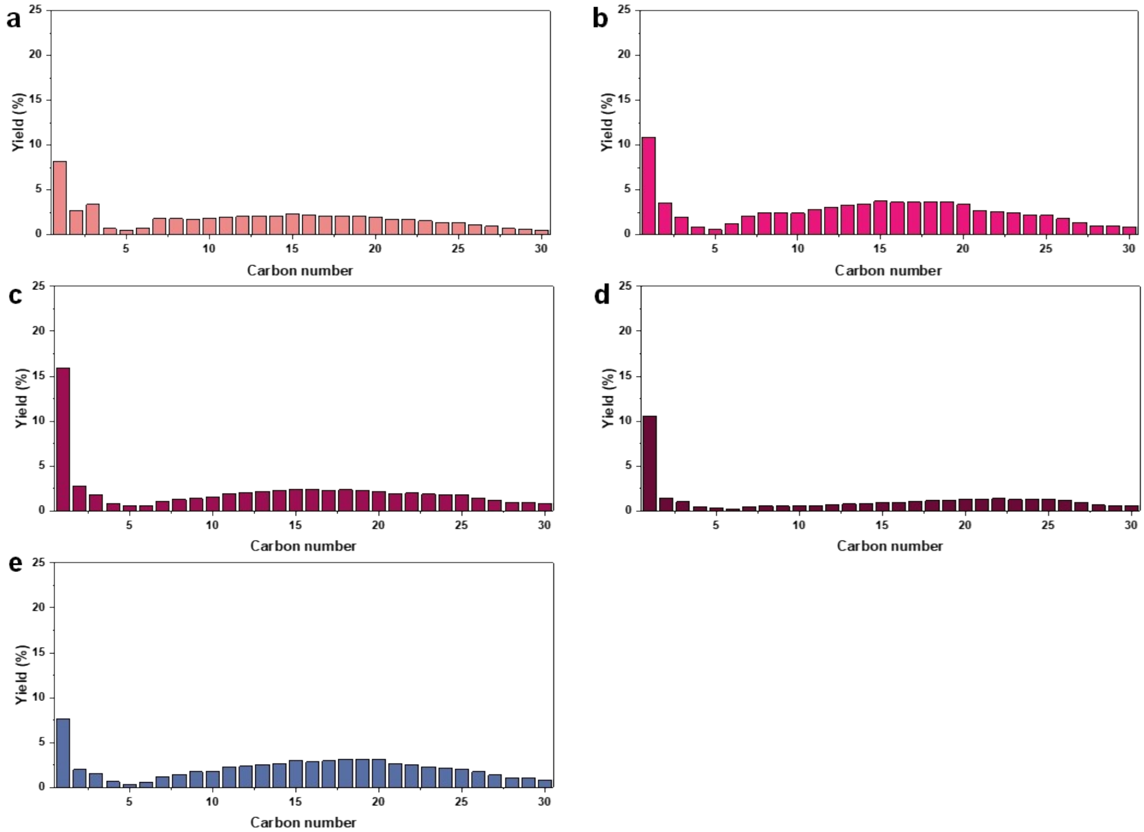

Fig. S13 Product distributions of PE hydrogenolysis over Ru/Al_2O_3 catalysts. (a) 0.5Ru/NA-Al_2O_3, (b) 1Ru/NA-Al_2O_3, (c) 5Ru/NA-Al_2O_3, (d) 8Ru/NA-Al_2O_3 and (e) 1Ru/*com*-Al_2O_3. Reaction conditions: 3.0 g PE, 1 mg Ru, 250 °C, 40 bar H_2, 2.5 h.

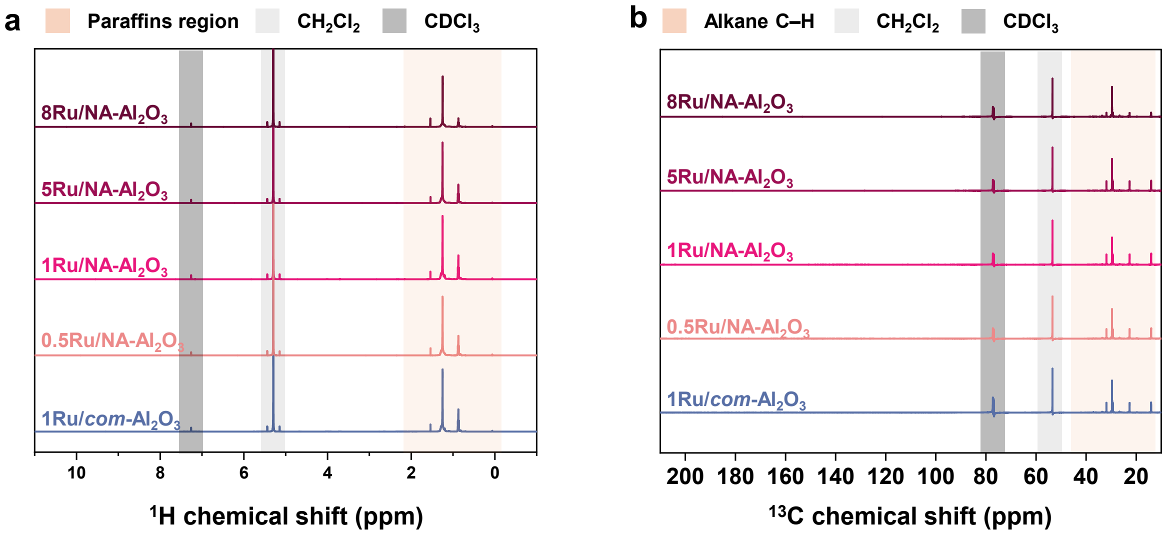

Fig. S14 (a) ^{1}H NMR and (d) ^{13}C NMR spectra of liquid/wax products (C_5–C_{30+}). The ^{1}H NMR region of paraffinic (orange), CH_2Cl_2 (gray), and $CDCl_3$ (dark gray) is highlighted. The ^{13}C NMR region of alkane C–H (orange), CH_2Cl_2 (gray), and $CDCl_3$ (dark gray) species is similary indicated. Reaction conditions: 3.0 g PE, 1 mg Ru, 250 °C, 40 bar H_2, 2.5 h.

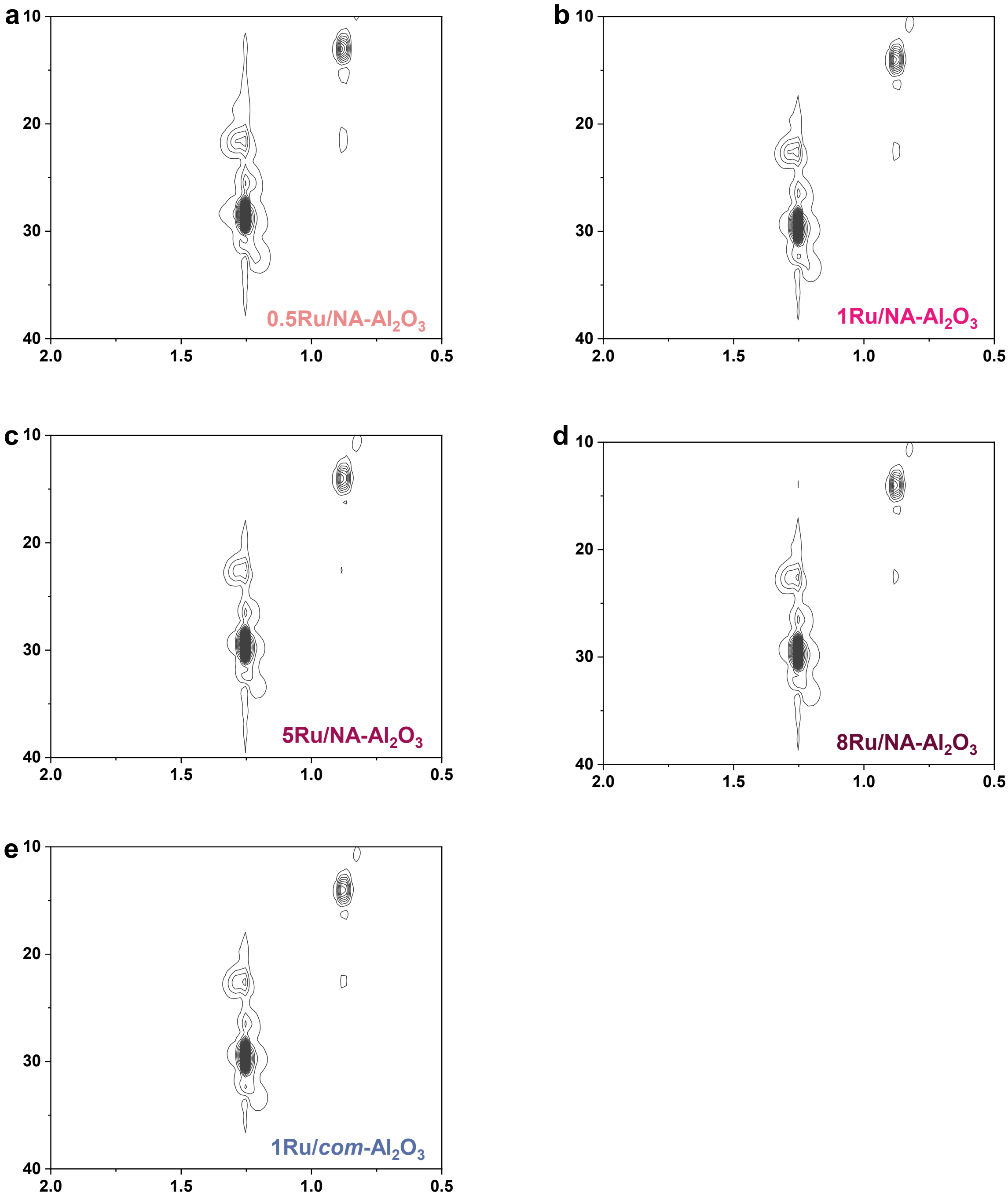

Fig. S15 2D-HSQC NMR spectra of liquid hydrocarbon products. (a) 0.5Ru/NA-Al_2O_3, (b) 1Ru/NA-Al_2O_3, (c) 5Ru/NA-Al_2O_3, (d) 8Ru/NA-Al_2O_3 and (e) 1Ru/*com*-Al_2O_3. The integrated region of *n*-paraffins CH CH groups is observed at ^{13}C (1.5–1.0 ppm).[1] No characteristic peaks were detected in regions corresponding to *iso*-alkanes (^{1}H (1.7–1.5 ppm); ^{13}C (30–27 ppm)) or aromatic compounds (^{1}H (1.5–1.3 ppm); ^{13}C (16–13 ppm)). Reaction conditions: 3.0 g PE, 1 mg Ru, 250 °C, 40 bar H_2, 2.5 h.

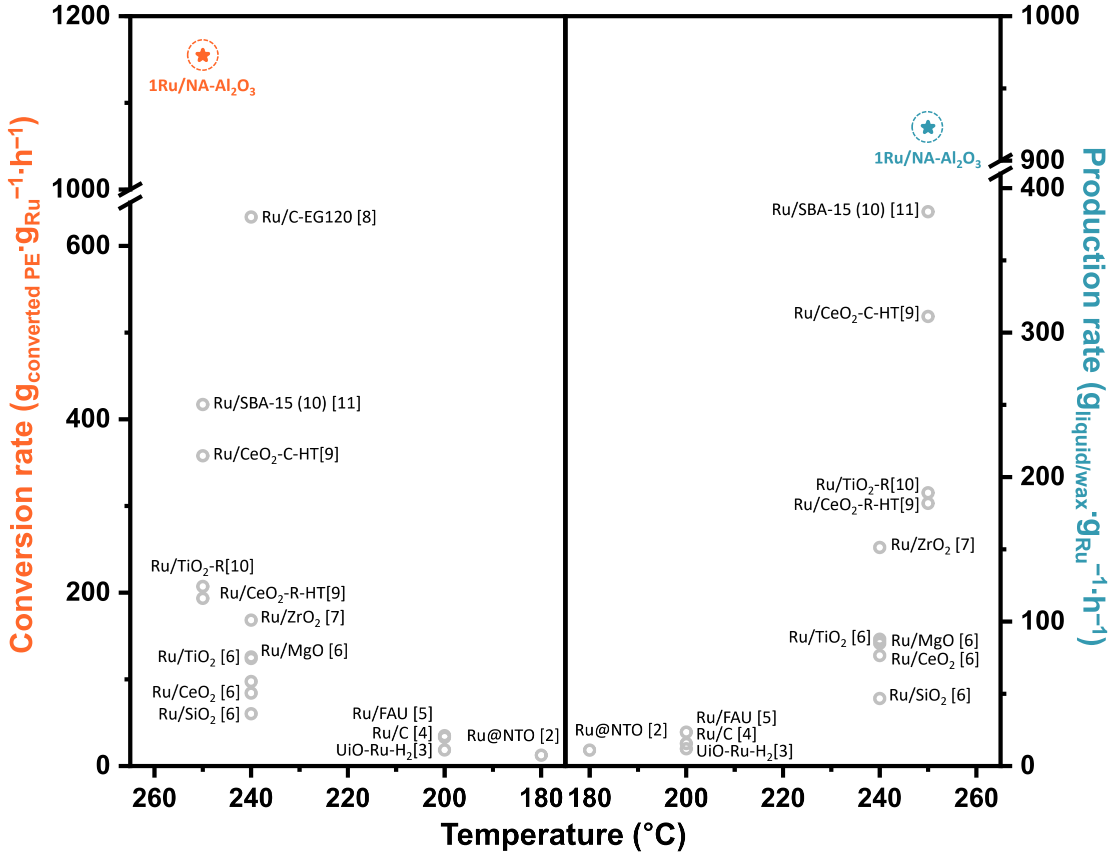

Fig. S16 Performance comparison of this work with reported Ru-based catalysts in the hydrogenolysis of PE (Mw ~4,000, Mn ~1,700).[2-11]

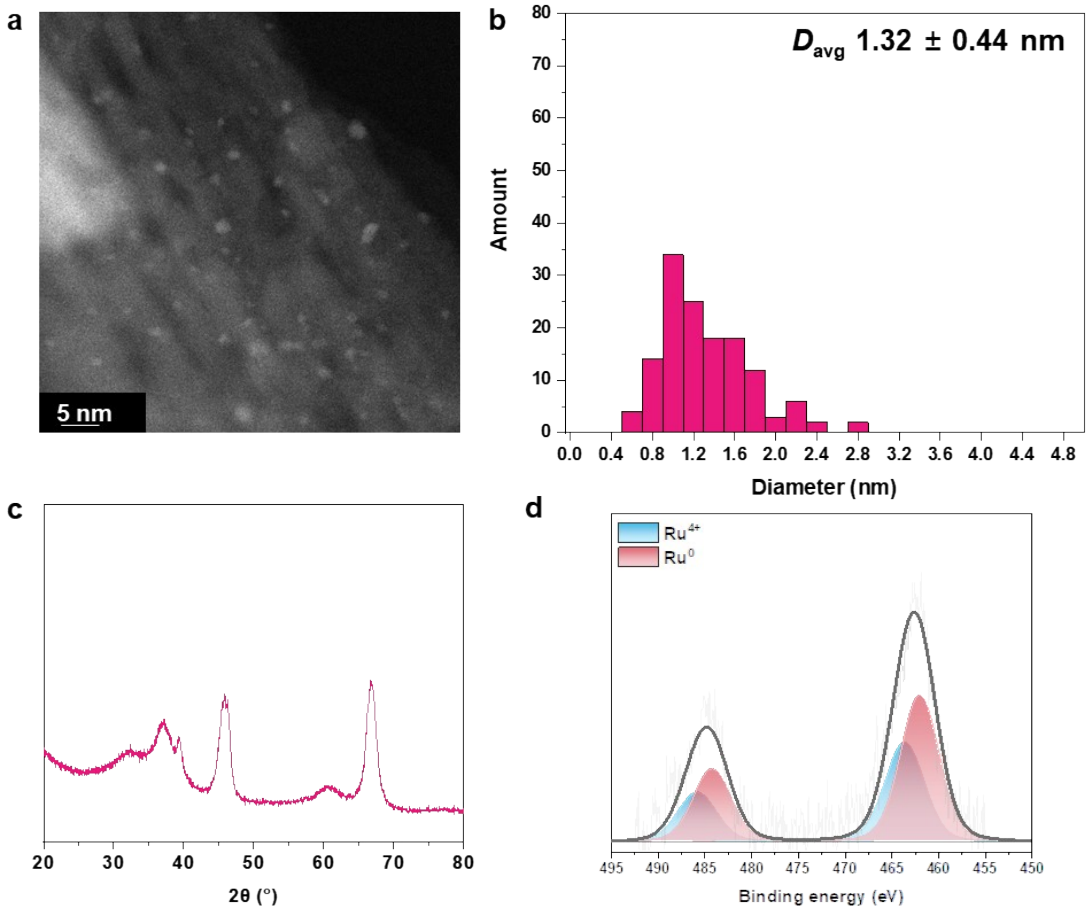

e

Catalyst	Ru (wt%)
1Ru/NA-Al_2O_3	0.98

Fig. S17 (a) HAADF-STEM images of 1Ru/NA-Al_2O_3 after PE hydrogenolysis reaction. (b) Particle size distribution of 1Ru/NA-Al_2O_3 after PE hydrogenolysis reaction. (c) XRD pattern of 1Ru/NA-Al_2O_3 after PE hydrogenolysis reaction. (d) XPS profiles of 1Ru/NA-Al_2O_3 after PE hydrogenolysis reaction. (e) Ru contents of 1Ru/NA-Al_2O_3 after PE hydrogenolysis reaction (analyzed by ICP-OES). Reaction conditions: 3.0 g PE (M_w ~4,000, M_n ~1,700), 1 mg Ru, 250 °C, 40 bar H_2, 2.5 h.

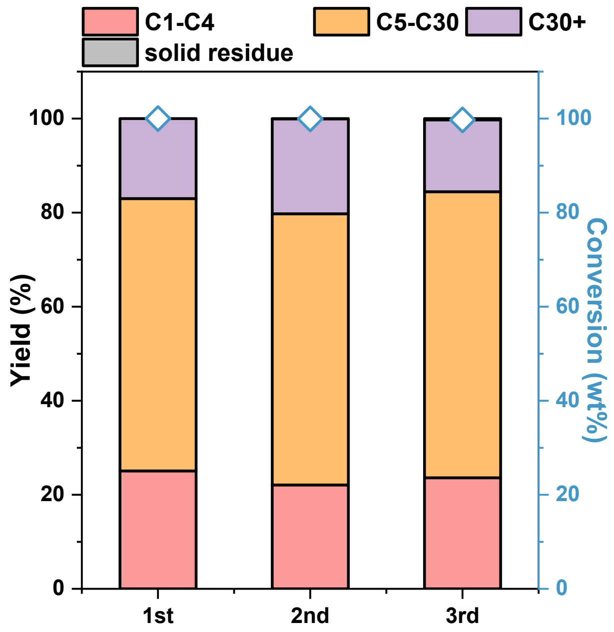

Fig. S18 Reusability test of 1Ru/NA-Al_2O_3 catalyst in PE hydrogenolysis. Reaction conditions: 3.0 g PE, 1 mg Ru, 280 °C, 40 bar H_2, 1 h.

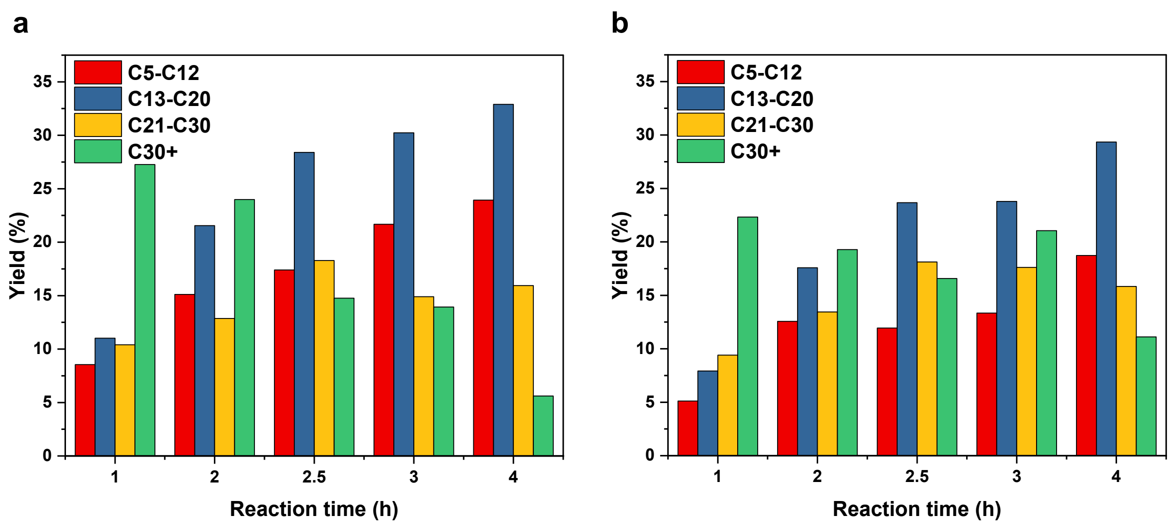

Fig. S19 Time-dependent product distributions for (a) 1Ru/NA-Al_2O_3 and (b) 1Ru/*com*-Al_2O_3 catalysts. Reaction conditions: 3.0 g PE (Mw ~4,000, Mn ~1,700), 1 mg Ru, 250 °C, 40 bar H_2.

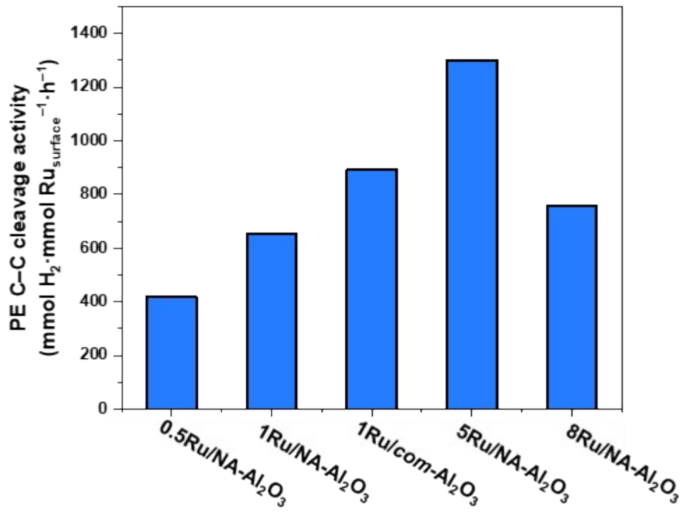

Fig. S20 PE C–C bond cleavage activity of catalysts. Reaction conditions: 3.0 g PE (M_w ~4,000, M_n ~1,700), 1 mg Ru, 250 °C, 40 bar H_2, and 2.5 h.

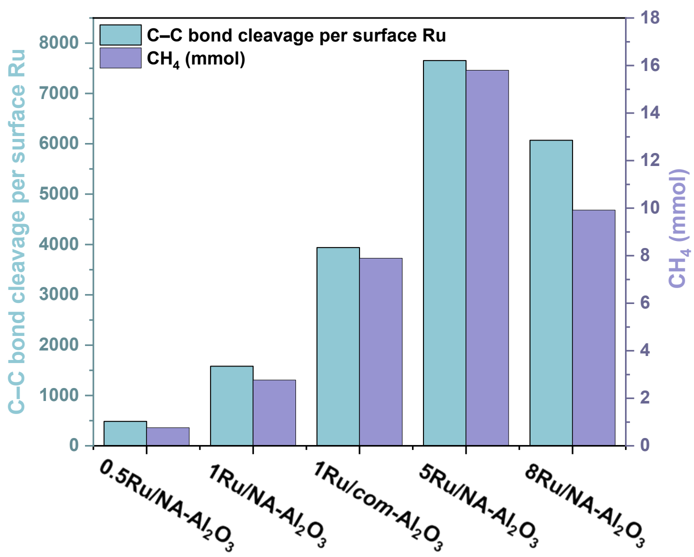

Fig. S21 C–C bond cleavage per surface Ru and methane production under same reaction conditions in $C_{18}H_{38}$ hydrogenolysis. Reaction conditions: 3.0 g $C_{18}H_{38}$, 0.5 mg Ru, 250 °C, 40 bar H_2, 20 min.

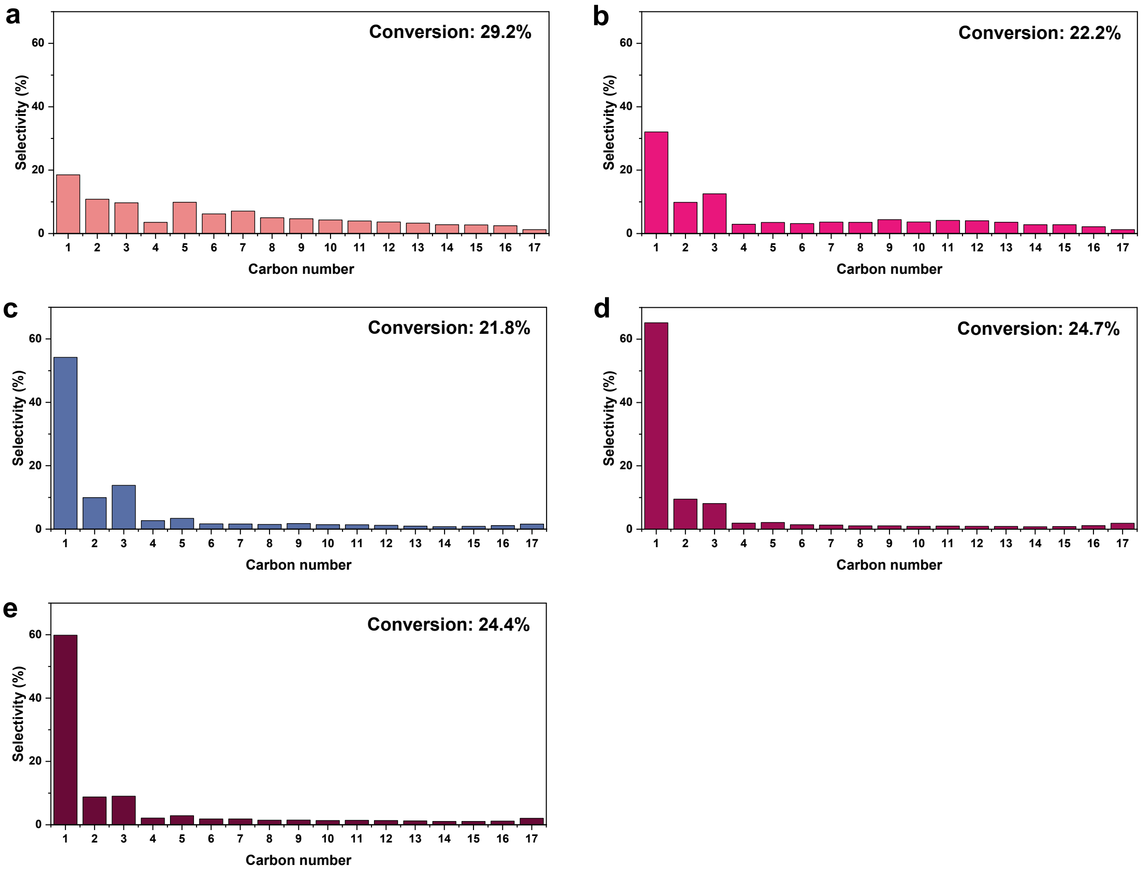

Fig. S22 Conversion (mol%) and product selectivity (mol%) of 0.5Ru/NA-Al_2O_3, (b) 1Ru/NA-Al_2O_3, (c) 1Ru/*com*-Al_2O_3, (d) 5Ru/NA-Al_2O_3, and (e) 8Ru/NA-Al_2O_3. Reaction conditions: 3.0 g $C_{18}H_{38}$, 0.5 mg Ru, 250 °C, 40 bar H_2. The reaction times were 30 min for 0.5Ru/NA-Al_2O_3, 20 min for 1Ru/NA-Al_2O_3 and 1Ru/*com*-Al_2O_3, and 10 min for 5Ru/NA-Al_2O_3 and 8Ru/NA-Al_2O_3.

Table S1. Physicochemical properties of as-prepared Ru/Al_2O_3 catalysts.

Catalyst	Ru (wt%)[a]	S_{BET} ($m^2 \cdot g^{-1}$) [b]	V_p ($cm^3 \cdot g^{-1}$) [c]	Pore size (nm)[c]
$0.5Ru/NA\text{-}Al_2O_3$	0.50	152.3	1.03	25.8
$1Ru/NA\text{-}Al_2O_3$	0.99	142.6	1.00	24.3
$5Ru/NA\text{-}Al_2O_3$	4.76	159.0	0.83	17.6
$8Ru/NA\text{-}Al_2O_3$	8.34	160.1	0.81	17.0
1Ru/*com*-Al_2O_3	0.88	183.8	0.45	8.2
NA-Al_2O_3	-	160.0	1.07	21.6
com-Al_2O_3	-	185.4	0.47	8.1

[a] Analyzed by ICP-OES.
[b] BET specific surface area.
[c] Calculated by BJH method.

Table S2. $Ru^{4+}/(Ru^0 + Ru^{4+})$ atomic ratios of as-prepared Ru/Al_2O_3 catalysts.

Catalyst	$Ru^{4+}/(Ru^0 + Ru^{4+})$ atomic ratio[a]
$0.5Ru/NA\text{-}Al_2O_3$	1
$1Ru/NA\text{-}Al_2O_3$	0.65
$5Ru/NA\text{-}Al_2O_3$	0.40
$8Ru/NA\text{-}Al_2O_3$	0.33
1Ru/*com*-Al_2O_3	0.59

[a] Analyzed by XPS

Table S3. Fitting parameters of Ru *K*-edge k^3-weighted EXAFS spectra of Ru/Al_2O_3 catalysts.

Sample	Path	CN[a]	R (Å)[b]	σ^2(Å^2)[c]	ΔE_0 (eV)[d]	R factor[e]
RuO_2	Ru–O	6	1.98	0.003	0.49	0.017
Ru foil	Ru–Ru	12	2.68	0.004	-4.47	0.004
1Ru/*com*-Al_2O_3	Ru–O	3.7	2.08	0.006	5.02	0.017
	Ru–Ru	2.6	2.71	0.011		
0.5Ru/NA-Al_2O_3	Ru–O	2.6	2.05	0.001	5.52	0.026
	Ru–Al	1.0	2.60	0.004		
1Ru/NA-Al_2O_3	Ru–O	2.7	2.06	0.004	3.34	0.027
	Ru–Al	1.0	2.55	0.012		
	Ru–Ru	2.3	2.70	0.013		
5Ru/NA-Al_2O_3	Ru–O	3.4	2.01	0.009	1.99	0.013
	Ru–Ru	3.3	2.70	0.008		
8Ru/NA-Al_2O_3	Ru–O	3.3	2.01	0.009	-1.25	0.013
	Ru–Ru	3.3	2.70	0.007		

[a] Coordination number.
[b] Bond distance.
[c] Debye–Waller coefficient.
[d] ΔE_0: Internal potential correction.
[e] R factor obtained from the best fit of each catalyst.

Table S4. Catalytic performance of Ru/Al_2O_3 catalysts in PE hydrogenolysis.

Catalyst	Time (h)	Conversion rate ($g_{converted\ PE}\cdot g_{Ru}^{-1}\cdot h^{-1}$)	Production rate ($g_{liquid/wax}\cdot g_{Ru}^{-1}\cdot h^{-1}$)	C1–C4 yield (%)	C5–C30 yield (%)	C30+ yield (%)	Conversion (%)	$C_{captured}$[c] (%)
$0.5Ru/NA\text{-}Al_2O_3$[a]	2.5	1.08×10^3	8.76×10^2	15.1	41.4	33.1	89.7	66.9
$1Ru/NA\text{-}Al_2O_3$[a]	1	2.08×10^3	1.68×10^3	12.0	30.0	27.3	69.2	72.7
$1Ru/NA\text{-}Al_2O_3$[a]	2	1.36×10^3	1.08×10^3	16.8	49.5	24.0	90.3	76.0
$1Ru/NA\text{-}Al_2O_3$[a]	2.5	1.15×10^3	9.23×10^2	17.4	64.1	14.8	96.2	85.2
$1Ru/NA\text{-}Al_2O_3$[a]	3	9.99×10^2	7.86×10^2	19.2	66.8	13.9	99.9	86.1
$1Ru/NA\text{-}Al_2O_3$[a]	4	7.50×10^2	5.72×10^2	21.6	72.8	5.6	100.0	94.4
$5Ru/NA\text{-}Al_2O_3$[a]	2.5	9.98×10^2	7.10×10^2	21.4	44.2	17.6	83.2	82.4
$8Ru/NA\text{-}Al_2O_3$[a]	2.5	6.60×10^2	4.77×10^2	13.5	23.4	18.1	55.0	81.9
1Ru/*com*-Al_2O_3[a]	1	1.58×10^3	1.32×10^3	8.0	22.4	22.3	52.7	77.7
1Ru/*com*-Al_2O_3[a]	2	1.10×10^3	9.25×10^2	10.8	43.6	19.3	73.6	80.7
1Ru/*com*-Al_2O_3[a]	2.5	9.87×10^2	8.28×10^2	11.9	53.7	16.6	82.3	83.4
1Ru/*com*-Al_2O_3[a]	3	9.56×10^2	7.34×10^2	19.8	54.7	21.1	95.6	79.0
1Ru/*com*-Al_2O_3[a]	4	7.50×10^2	5.43×10^2	25.0	63.9	11.1	100.0	88.9
$1Ru/NA\text{-}Al_2O_3$[b]	2	3.91×10^2	2.87×10^2	6.2	6.8	13.1	26.1	86.9
$1Ru/NA\text{-}Al_2O_3$[b]	4	4.90×10^2	3.69×10^2	14.6	25.4	25.3	65.3	74.7
$1Ru/NA\text{-}Al_2O_3$[b]	6	4.45×10^2	3.56×10^2	16.1	51.3	21.6	88.9	78.4
1Ru/*com*-Al_2O_3[b]	2	1.22×10^2	55.6	4.0	2.2	1.9	8.1	98.1
1Ru/*com*-Al_2O_3[b]	4	2.36×10^2	1.76×10^2	6.8	6.3	18.4	31.5	81.6
1Ru/*com*-Al_2O_3[b]	6	3.73×10^2	2.85×10^2	15.9	35.5	23.2	74.5	76.8

[a] Reaction conditions: 3.0 g PE (Mw ~4,000, Mn ~1,700), 1 mg Ru, 250 °C, 40 bar H_2.
[b] Reaction conditions: 3.0 g PE (Mw ~4,000, Mn ~1,700), 1 mg Ru, 220 °C, 40 bar H_2.

[c] $C_{captured}\,(\%) = \frac{C_{C1\text{–}C4} + C_{C5\text{–}C30} + C_{solid}}{C_{initial}} \times 100$, where $C_{initial}$ is the initial substrate's amount (in C-mol) and $C_{C1\text{–}C4}$, $C_{C5\text{–}C30}$, and C_{solid} are the amount of C1–C4, C5–C30, and solid residue (in C-mol),

respectively.

Table S5. *Iso*-alkane composition in the C_{10} Product (based on GC analysis). Reaction conditions: 3.0 g PE, 1 mg Ru, 250 °C, 40 bar H_2, 2.5 h.

Catalyst	*Iso*-alkane fraction[a]
0.5Ru/NA-Al_2O_3	0.10
1Ru/NA-Al_2O_3	0.10
5Ru/NA-Al_2O_3	0.10
8Ru/NA-Al_2O_3	0.09
1Ru/*com*-Al_2O_3	0.10

[a] *Iso*-alkane fraction = $\frac{\text{i - C10 product (mmol)}}{\text{Total C10 product (mmol)}}$

Table S6. Comparison of conversion and production rates in the hydrogenolysis of PE (M_w ~4,000, M_n ~1,700) using reported Ru-based catalysts.

Catalyst	Temperature (°C)	Time (h)	Conversion rate ($g_{converted\ PE} \cdot g_{Ru}^{-1} \cdot h^{-1}$)	Production rate ($g_{liquid/wax} \cdot g_{Ru}^{-1} \cdot h^{-1}$) (Carbon number)	Ref
1Ru/NA-Al_2O_3	250	2.5	1.15×10^3	9.23×10^2 (C5-C30+)	This work
Ru@NTO-NH	180	8	12.5	11.0 (C6-C35)	[2]
UiO-66-RuH_2	200	72	18.6	12.1 (C5-C35)	[3]
Ru/C	200	16	33.3	15.6 (C8-C45)	[4]
Ru/FAU	200	16	35.0	23.5 (C5-C33)	[5]
Ru/MgO	240	4	1.26×10^2	85.0 (C5-C45)	[6]
Ru/TiO_2			1.24×10^2	86.7 (C5-C45)	
Ru/CeO_2	240	8	84.2	76.5 (C5-C45)	
Ru/SiO_2			60.4	46.8 (C5-C45)	
Ru/ZrO_2	240	4	1.68×10^2	1.51×10^2 (C5-C45)	[7]
Ru/C-EG120	240	1.5	6.09×10^2	-	[8]
Ru/CeO_2-R-HT	250	2	1.93×10^2	1.82×10^2 (C5-C41)	[9]
Ru/CeO_2-C-HT			3.58×10^2	3.11×10^2 (C5-C41)	
Ru/TiO_2-R	250	3	2.07×10^2	1.89×10^2 (C5-C40)	[10]
Ru/SBA-15 (10)	250	1.5	4.17×10^2	3.84×10^2 (C5-C40)	[11]

Table S7. Comparison of conversion and product yield in the hydrogenolysis of PE (M_w ~4,000, M_n ~1,700) using reported Ru-based catalysts.

Catalyst	Temperature (°C)	Time (h)	Conversion (%)	Gas (%) (Carbon number)	Liquid/Wax (%) (Carbon number)	Ref
$1Ru/NA-Al_2O_3$	250	2.5	96.2	19.3 (C1-C4)	76.9 (C5-C30+)	This work
Ru@NTO-NH	180	8	100	12 (C1-C5)	88 (C6-C35)	[2]
UiO-66-RuH_2	200	72	90	32 (C1-C4)	58 (C5-C35)	[3]
Ru/C	200	16	95	45 (C1-C7)	50 (C8-C45)	[4]
Ru/FAU	200	16	100	33 (C1-C5)	67 (C5-C33)	[5]
Ru/MgO	240	4	74	24 (C1-C4)	50 (C5-C45)	[6]
Ru/TiO_2			73	22 (C1-C4)	51 (C5-C45)	
Ru/CeO_2	240	8	99	10 (C1-C4)	90 (C5-C45)	
Ru/SiO_2			71	15 (C1-C4)	55 (C5-C45)	
Ru/ZrO_2	240	4	99	11 (C1-C4)	89 (C5-C45)	[7]
Ru/C-EG120	240	1.5	95	-	-	[8]
Ru/CeO_2-R-HT	250	2	53	3 (C1-C4)	50 (C5-C41)	[9]
Ru/CeO_2-C-HT			93	13 (C1-C4)	81 (C5-C41)	
Ru/TiO_2-R	250	3	91	8 (C1-C4)	84 (C5-C40)	[10]
Ru/SBA-15 (10)	250	1.5	92	7 (C1-C4)	85 (C5-C40)	[11]

References

1. H. Lee, C. Hur, Y. H. Lee, J. W. Moon, H. Lee, T. H. Kim, D. Oh, J.-S. Bae, W.-H. Kim and K. An, *ACS Catal.*, 2024, **14**, 12744-12756.
2. X. Zhang, Q. Gan, P. Zhou, Z. Chen, Z. Zhang and G.-P. Lu, *Appl. Catal., B*, 2024, **344**, 123626.
3. M. Chauhan, N. Antil, B. Rana, N. Akhtar, C. Thadhani, W. Begum and K. Manna, *JACS Au*, 2023, **3**, 3473-3484.
4. J. E. Rorrer, G. T. Beckham and Y. Román-Leshkov, *Jacs Au*, 2020, **1**, 8-12.
5. J. E. Rorrer, A. M. Ebrahim, Y. Questell-Santiago, J. Zhu, C. Troyano-Valls, A. S. Asundi, A. E. Brenner, S. R. Bare, C. J. Tassone, G. T. Beckham, and Y. Román-Leshkov, *ACS Catal.*, 2022, **12**, 13969-13979.
6. Y. Nakaji, M. Tamura, S. Miyaoka, S. Kumagai, M. Tanji, Y. Nakagawa, T. Yoshioka and K. Tomishige, *Appl. Catal., B*, 2021, **285**, 119805.
7. M. Tamura, S. Miyaoka, Y. Nakaji, M. Tanji, S. Kumagai, Y. Nakagawa, T. Yoshioka and K. Tomishige, *Appl. Catal., B*, 2022, **318**, 121870.
8. P. Hu, C. Zhang, M. Chu, X. Wang, L. Wang, Y. Li, T. Yan, L. Zhang, Z. Ding, M. Cao, P. Xu, Y. Li, Y. Cui, Q. Zhang, J. Chen and L. Chi, *J. Am. Chem. Soc.*, 2024, **146**, 7076-7087.
9. A. Buhori, J.-W. Choi, H. Lee, C. S. Kim, K. H. Kim, K. Kim, W. Yang, J.-M. Ha and C.-J. Yoo, *Chem. Eng. J.*, 2024, **499**, 156097.
10. T. Kim, H. Nguyen-Phu, T. Kwon, K. H. Kang and I. Ro, *Environ. Pollut.*, 2023, **331**, 121876.
11. H. Nguyen-Phu, T. Kwon, T. Kim, L. T. Do, K. H. Kang and I. Ro, *Chem. Eng. J.*, 2023, **475**, 146076.